

Role of native point defects and Hg impurities in the electronic properties of Bi₄I₄

Gustavo H. Cassemiro,¹ C. David Hinojosa,² Leandro Rodrigues de Faria,³ Daniel A. Mayoh,⁴ Maria C. O. Aguiar,¹ Martin R. Lees,⁴ Geetha Balakrishnan,⁴ J. Larrea Jiménez,² Antonio Jefferson da Silva Machado,³ Valentina Martelli,² and Walber H. Brito¹

¹*Departamento de Física, Universidade Federal de Minas Gerais,
C. P. 702, 30123-970, Belo Horizonte, MG, Brazil*

²*Laboratory for Quantum Matter under Extreme Conditions,
Instituto de Física, Universidade de São Paulo, 05508-090, São Paulo, Brazil*

³*Escola de Engenharia de Lorena - DEMAR, Universidade de São Paulo, 12612-550, Lorena, Brazil*

⁴*Department of Physics, University of Warwick, Coventry CV4 7AL, United Kingdom*

(Dated: October 25, 2024)

We studied the effects of point defects and Hg impurities in the electronic properties of bismuth iodide (Bi₄I₄). Our transport measurements after annealing at different temperatures show that the resistivity of Bi₄I₄ depends on its thermal history, suggesting that the formation of native defects and impurities can shape the temperature dependence of electrical resistivity. Our density functional theory calculations indicate that the bismuth and iodine antisites, and bismuth vacancies are the dominant native point defects. We find that bismuth antisites introduce resonant states in the band-edges, while iodine antisites and bismuth vacancies lead to a *n*-type and *p*-type doping of Bi₄I₄, respectively. The Hg impurities are likely to be found at Bi substitutional sites, giving rise to the *p*-type doping of Bi₄I₄. Overall, our findings indicate that the presence of native point defects and impurities can significantly modify the electronic properties, and, thus, impact the resistivity profile of Bi₄I₄ due to modifications in the amount and type of carriers, and the associated defect(impurity) scattering. Our results suggest possible routes for pursuing fine-tuning of the electronic properties of quasi-one-dimensional quantum materials.

I. Introduction

The quasi-one dimensional bismuth halogenides have attracted the attention of the scientific community due to their emerging quantum properties, such as superconductivity and non-trivial topology [1]. Among this family of compounds, bismuth iodide (Bi₄I₄) and bismuth bromide (Bi₄Br₄) were proposed to host weak, strong, or high-order topological insulating phases as well as pressure-induced superconductivity, depending on the crystal structure [2–4].

In both Bi₄I₄ and Bi₄Br₄, the molecular chains can stack in two distinct forms, giving rise to the so-called α and β phases. More interestingly, these compounds can be viewed as controlled platforms where one can go from one phase to another by tuning the temperature. In the case of Bi₄I₄, this temperature-driven first-order phase transition takes place around $T_C \approx 300$ K [4]. For $T > 300$ K, Bi₄I₄ crystallizes in the β phase, which has been reported to host a non-trivial topological phase. Density functional theory (DFT) and GW calculations have indicated that the β phase is a weak topological insulator [2, 5], which was validated by angle-resolved photoemission spectroscopy [2]. Regarding the α phase, which occurs for $T < 300$ K, it was earlier reported as a trivial insulator according to the Z_2 criterion. However, more recent studies found evidence of its high-order topological character [3], dictated by low-energy electronic states originating mostly from the bismuth *p*-orbitals [5].

The complex interplay between the topological phases and superconductivity was explored in bismuth

halogenides using external pressure as a tuning parameter. For Bi₄Br₄, it was found that the non-trivial topological phase is robust at higher pressures, indicating a possible coexistence between superconductivity and topology [6]. Moreover, in the work of Qi and coworkers [7], it was found that Bi₄I₄ undergoes multiple topological phase transitions before entering into the superconducting phase. In addition, it was found that Bi₄I₄ undergoes several structural transitions with the increasing of pressure, from monoclinic ($C2/m$) to trigonal ($P31c$), and then from the trigonal to a tetragonal ($P4/mmm$) structure [8].

The investigation of quantum oscillations in electrical transport pointed out the existence of 2D or 3D Fermi surfaces in α -Bi₄I₄ for *n* and *p*-doped samples, respectively [9]. A 3D Fermi surface was also revealed for the β -Bi₄I₄, for magnetic fields below 15.9 T, where there is a near metal to insulator transition [10]. Although those works indicated that defects and impurities might have an important role, their impact on the electronic structure has not been reported yet. Mu *et al.* [11] reported that complex hollow-type defects, which appear in the regions of α and β phase separation, modulate the density of states of Bi₄I₄, which might explain the sample-dependence observed in the resistivity measurements. In our recent work, we pointed out that simple native defects can be the source of the instability of the β phase at low temperatures after quenching [12], suggesting that it is not the different topology of the phase that rules the observed temperature evolution of the resistivity, shedding some light on the source of the rather confusing resistivity measurements reported so far

for the two phases when it come to the comparison of the temperature-dependence that does not seem to be ruled by the different topological phase.

Although Bi_4I_4 has been intensively studied in the last few years, there is a lack of a systematic study about the effects of native point defects and impurities on the electronic properties of both α and β phases. We emphasize that scrutinizing the presence of different defects, which are intrinsic to all samples, may help to understand the wide variety of resistivity profiles which are impacted by intrinsic and extrinsic doping and the appearance of defect/impurity electronic states, and to avoid misleading interpretation related to the expected electronic properties stemming from a specific topological phase. In this work, we focus on the effects of native defects and Hg impurities on the electronic properties of both α and β phases of Bi_4I_4 . In particular, we have addressed the formation energies and electronic structure of native point defects and mercury (Hg) impurities in Bi_4I_4 . Hg impurities were considered due to possible contamination of samples during the Bi_4I_4 synthesis. The presence of Hg is experimentally observed on the crystal surface of our samples by energy-dispersive x-ray spectroscopy (EDX) investigation.

We find that bismuth antisites are the dominant native defects, followed by iodine antisites and bismuth vacancies. More importantly, we observe that bismuth antisites do not dope the system, while iodine antisites and vacancies lead to n and p -type doping of Bi_4I_4 , respectively. The Hg antisites act like p dopants. Overall, our calculations show that energetically stable point defects and Hg impurities modify the amount of carriers in Bi_4I_4 , introduce additional scattering states around the Fermi energy, and may have significant effects on the resistivity of Bi_4I_4 at low-temperatures. Thus, the analysis of the features observed in electrical transport experiments of Bi_4I_4 as a consequence of a specific topological phase should consider these findings to avoid misleading interpretations.

Our paper is organized in three sections. In Sec. II, we present the employed experimental and theoretical methods. The EDX and resistivity measurements are discussed in Sec. III A. The formation energies of the investigated defects and impurities are discussed in Sec. III B and III C, and their effects on the electronic structure are discussed in Sec. III D. Our conclusions are summarized in Sec. IV.

II. Experimental and Computational Methods

α - Bi_4I_4 single crystals were grown by chemical vapor transport as explained in Ref. [12]. For the thermal treatment samples were annealed for 24 hrs at 50 °C and 100 °C, and cooled slowly to smoothly recover the α phase, in contrast to what we reported in [12] where a rapid quenching aimed at stabilizing a metastable β -phase at low temperature. EDX was used on a scanning

electron microscope (SEM) for the compositional analysis of the synthesized crystals to check the stoichiometry and the presence of other atomic elements. Electrical resistivity measurements were performed using an Advanced Research System DE-202N cryocooler and a Quantum Design - Physical Property Measurement System in a 4-point configuration. Electrical contacts on the samples were made using gold wires fixed with silver paint on Pt electrodes previously deposited on the surface to minimize the contact resistance.

Our first-principles calculations were performed within the density functional theory as implemented in the Vienna *ab initio* simulation package (VASP) [13, 14]. The Perdew-Burke-Ernzerhof generalized gradient approximation (PBE-GGA) was used to perform the calculations. However, this functional cannot describe the van der Waals interactions presented in Bi_4I_4 , so the dispersion correction (vdW-DF) [15] was employed. The spin-polarized and spin-orbit coupling (SOC) were also considered in our calculations. In addition, we employed projector augmented wave (PAW) [16] potentials, and we relaxed the structures until the forces on each atom were < 0.01 eV/Å and total energies converged within a 1×10^{-6} eV criterion. We used an energy cutoff of 400 eV for the plane-wave basis. The total energies were calculated using a k -point mesh of $4 \times 3 \times 4$ for the α phase and $4 \times 3 \times 2$ for the β phase. The supercell approximation was employed to investigate the energetics and electronic properties of Bi_4I_4 in the presence of native defects and Hg impurities.

The relative equilibrium concentration of defects in the system depends on their formation energies, which can be obtained from the DFT total energies as follows [17, 18],

$$E^f(S_L) = [E_{\text{tot}}(S_L) - E_{\text{tot}}(\text{pristine})] - \sum_i n_i \mu_i, \quad (1)$$

where $E_{\text{tot}}(S_L)$ and $E_{\text{tot}}(\text{pristine})$ are the total energies of supercells with the presence of defect S_L (Kröger-Vink notation) and without the presence of defects, respectively. n_i is the number of species i that is added to ($n_i > 0$) or removed from ($n_i < 0$) the supercell to form the defect S_L . μ_i are the chemical potentials of different atomic species exchanged with their respective atomic reservoirs, obtained with reference to the calculated reference energies μ_i^0 , so $\mu_i = \mu_i^0 + \Delta\mu_i$. The values of $\Delta\mu_i$ depend on the environmental conditions in thermodynamic equilibrium. Due to the small band gaps of α and β phases we considered only neutral charge defects and impurities [2, 5].

III. Results and Discussions

A. EDX and resistivity measurements

In Fig. 1 we show the SEM image of one representative Bi_4I_4 sample. Compositional analysis has been done by

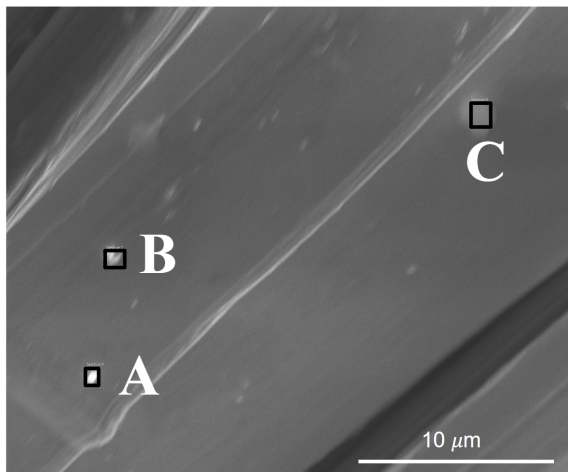


FIG. 1: SEM image of one representative Bi_4I_4 sample. Chemical composition was measured in the areas enclosed by numbered squares by EDX. The elemental composition is given in Table I.

EDX analysis across selected areas of the single crystal shown in Fig. 1 and are presented in Table I. The observed presence of Hg impurities on the surface and the similar ionic radius of Bi (117 pm) and Hg (114 pm) [19] suggest the possibility of Hg substitution in the bismuth site, although the evidence is not conclusive.

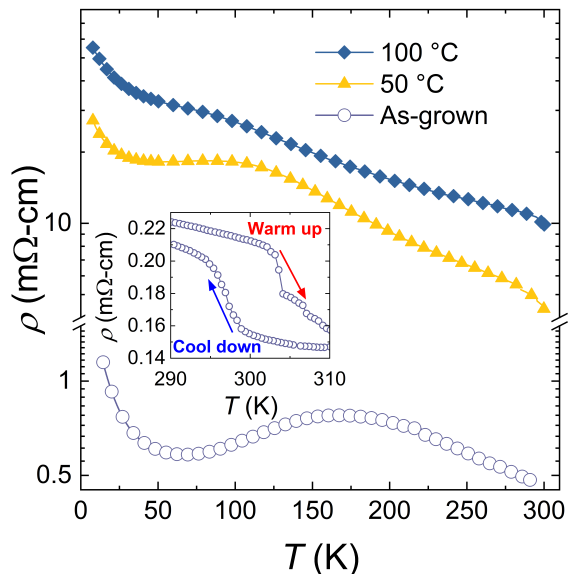


FIG. 2: Temperature dependence of the electrical resistivity of $\alpha\text{-Bi}_4\text{I}_4$ samples. Filled symbols correspond to samples annealed for one day, while open circles to the as-grown sample. The inset shows the hysteresis curve, indicating the phase transition.

The temperature dependence of electrical resistivity on selected samples of Bi_4I_4 after annealing at different temperatures is depicted in Fig. 2. In our previous work [12], we scrutinized the large variety of reported

TABLE I: Composition measured by EDX across areas indicated in Fig. 1. The expected nominal composition of the single crystals is 50:50 for Bi:I.

spectrum label	I (%)	Bi (%)	Hg (%)
A	66.49(3)	33.51(2)	-
B	66.61(3)	34.39(2)	-
C	49.14(2)	46.61(2)	4.25(2)

electrical resistivity of this compound. We observed that the temperature dependence does not seem to correlate with the topological (structural) phase. However, a direct comparison among the available data was not possible, as the growth processes, annealing, and quenching temperatures vary across the reported works. Here, we systematically investigated the temperature dependence of the electrical resistivity of Bi_4I_4 samples from the same batch, just annealing them at different temperatures. We confirm (see inset of Fig. 2) that there is the expected hysteresis across the structural transition temperature. A smooth crossing through T_C avoids phase coexistence for higher ($T > 310$ K) and lower temperatures ($T < 290$ K). Additionally, Fig. 2 shows a clear change of both the absolute value and of the temperature dependence of electrical resistivity in the α -phase after the annealing process; electrical resistivity increases by over one order of magnitude at room temperature after annealing. This feature suggests that the change in charge carrier density and additional scattering associated with the formation of native defects and impurities due to the samples' thermal history can likely be the source of the reduced conductivity. This evidence suggests that native defects and impurities have an important role: their presence can shape electronic properties within the same topological phase and will be analyzed and discussed in the following sections.

B. Defect-formation energies under distinct growth conditions

We first investigate the energetics of different types of native defects which may appear in Bi_4I_4 under Bi-rich and poor conditions. In particular, we have considered bismuth (Bi_I) and iodine (I_{Bi}) antisites, bismuth (Bi_i) and iodine (I_i) interstitials, and finally bismuth (V_{Bi}) and iodine (V_I) vacancies. We have considered all the possible interstitial and substitutional sites, labeled as A, B, and C in the α phase; A', B', C', D' in the β phase. The defects were introduced in ideal $3 \times 1 \times 2$ (96 atoms) and $3 \times 2 \times 3$ (144 atoms) supercells for α and β phases, respectively. In our previous work, we only obtained the formation energies of these defects under Bi-rich conditions [12]. In this work, we considered distinct chemical conditions as well as the existence of competing phases, as will be described below, to provide insights

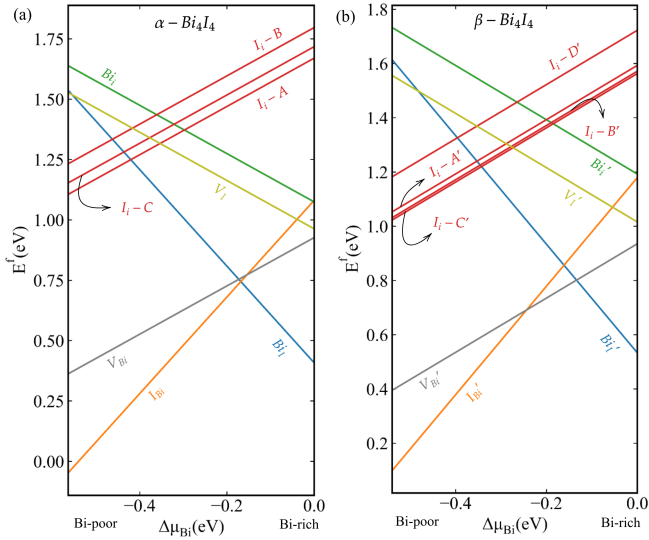


FIG. 3: Formation energies of neutral native defects, as a function of chemical potential $\Delta\mu_{\text{Bi}}$ for the (a) α and (b) β phases. Here, the Kröger-Vink notation is adopted.

on the relation between growth conditions and resulting electronic properties.

As can be seen in Eq. 1, the formation energy is a function of the atomic chemical potentials μ_i , representing the relative abundance of Bi and I species in the growth conditions. We evaluated the chemical potentials μ_{Bi} and μ_{I} in distinct limits to consider the different growth conditions. In a Bi-rich condition, $\mu_{\text{Bi}}^{\text{rich}}$ is calculated from the bulk bismuth, which exhibits $P2_1/m$ symmetry. Therefore, from the thermodynamic equilibrium condition, $\mu_{\text{I}}^{\text{poor}} = (\mu_{\text{Bi}_4\text{I}_4} - 4\mu_{\text{Bi}}^{\text{rich}})/4$, where $\mu_{\text{Bi}_4\text{I}_4}$ is the calculated total energy per formula unit. On the other hand, in I-rich conditions, $\mu_{\text{I}}^{\text{rich}}$ is obtained from the bulk iodine, which exhibits $Cmce$ symmetry. In this condition $\mu_{\text{Bi}}^{\text{poor}} = (\mu_{\text{Bi}_4\text{I}_4} - 4\mu_{\text{I}}^{\text{rich}})/4$.

In table II, we summarize the obtained formation energies for the native defects in both the α and β phases for Bi-rich (I-poor) and Bi-poor (I-rich) conditions. Values with an star were reported in our previous work [12]. The variation of the formation energies as a function of $\Delta\mu_{\text{Bi}} = \mu_{\text{Bi}}^{\text{poor}} - \mu_{\text{Bi}}^{\text{rich}}$ is shown in Fig. 3. As expected, we obtain similar formation energies of defects in the α and β phases, indicating that the concentration of neutral point defects is roughly independent of the Bi_4I_4 crystal structure. We also observe that bismuth and iodine interstitials have higher formation energies than the other native defects and are thus expected to appear in small concentrations. More importantly, our findings suggest that the bismuth antisites have low formation energies under Bi-rich conditions, followed by the bismuth and iodine vacancies. The relaxed structures of bismuth antisites in α (Bi_{I}) and β (Bi'_{I}) phases are shown in Figs. 4(a) and 5(a), respectively. The surrounding atoms are denoted by Bi1, Bi2, Bi3, and Bi4 in our relaxed structures. We find $\text{Bi}_{\text{I}}\text{-Bi}$ bond lengths of

3.05 and 3.75 Å in the α phase, and of 3.02 and 3.56 Å in the β phase. These findings indicate that Bi-antisites tend to modify the interactions between chains in both phases of Bi_4I_4 . In the pristine systems, the Bi3-I bond length is around 3.13 (3.11) Å in $\alpha(\beta)$ phase, while Bi1-I is around 3.76 (3.84) Å in the $\alpha(\beta)$ phase. In the case of bismuth vacancies, we do not observe any strong modification in the structures, as shown in Figs. 4(c) and 5(c), with Bi1-Bi2 bond lengths of around 8.4 Å in both phases. In pristine α and β phases the corresponding distance is around 8.4 Å.

For comparison, in the case of iodine interstitials in the α phase, the formation energy difference is $\Delta E^f = 1.26$ eV concerning the bismuth antisites. Regarding the vacancies, we find that iodine vacancies have higher formation energies than bismuth vacancies. Therefore, our findings suggest that the neutral charge Bi-antisites (Bi_{I}) and vacancies (V_{Bi}) are expected to be the dominant defects in Bi_4I_4 under Bi-rich conditions. We mention that recent scanning tunneling microscopy measurements observed the presence of Bi-vacancies in monolayers of Bi_4I_4 [11].

TABLE II: Formation energies (eV), E^f , of neutral native defects in α and β - Bi_4I_4 for Bi-rich (I-poor) and Bi-poor (I-rich) conditions. Values with a star were reported previously in Ref. [12].

System	Defect	E^f (eV) Bi-rich	E^f (eV) Bi-poor
α - Bi_4I_4	Bi_{I}	0.41*	1.54
	I_{Bi}	1.08*	-0.05
	Bi_i	1.07*	1.64
	$\text{I}_i\text{-A}$	1.67*	1.11
	$\text{I}_i\text{-B}$	1.80*	1.23
	$\text{I}_i\text{-C}$	1.72*	1.15
	V_{Bi}	0.93*	0.36
β - Bi_4I_4	V_{I}	0.96*	1.53
	Bi'_{I}	0.53*	1.61
	$\text{I}_{\text{Bi}}\text{-A}'$	1.18*	0.10
	$\text{I}_{\text{Bi}}\text{-B}'$	1.72	0.64
	Bi'_i	1.19*	1.73
	$\text{I}_i\text{-A}'$	1.59*	1.05
	$\text{I}_i\text{-B}'$	1.57*	1.03
	$\text{I}_i\text{-C}'$	1.56*	1.02
	$\text{I}_i\text{-D}'$	1.72*	1.18
	V'_{Bi}	0.94*	0.39
V'_{I}	1.02*	1.56	

On the other hand, in a bismuth-poor (I-rich) environment we observe a distinct feature. In this limit the iodine antisites (I_{Bi} and $\text{I}_{\text{Bi}} - \text{A}'$ in Table. II) are preferred due to their low formation energies, as emphasized by $E^f = -0.05$ eV (0.10 eV) in the α (β) phase. As a result, our findings suggest that this type of defect should be the dominant native defect in Bi_4I_4 under

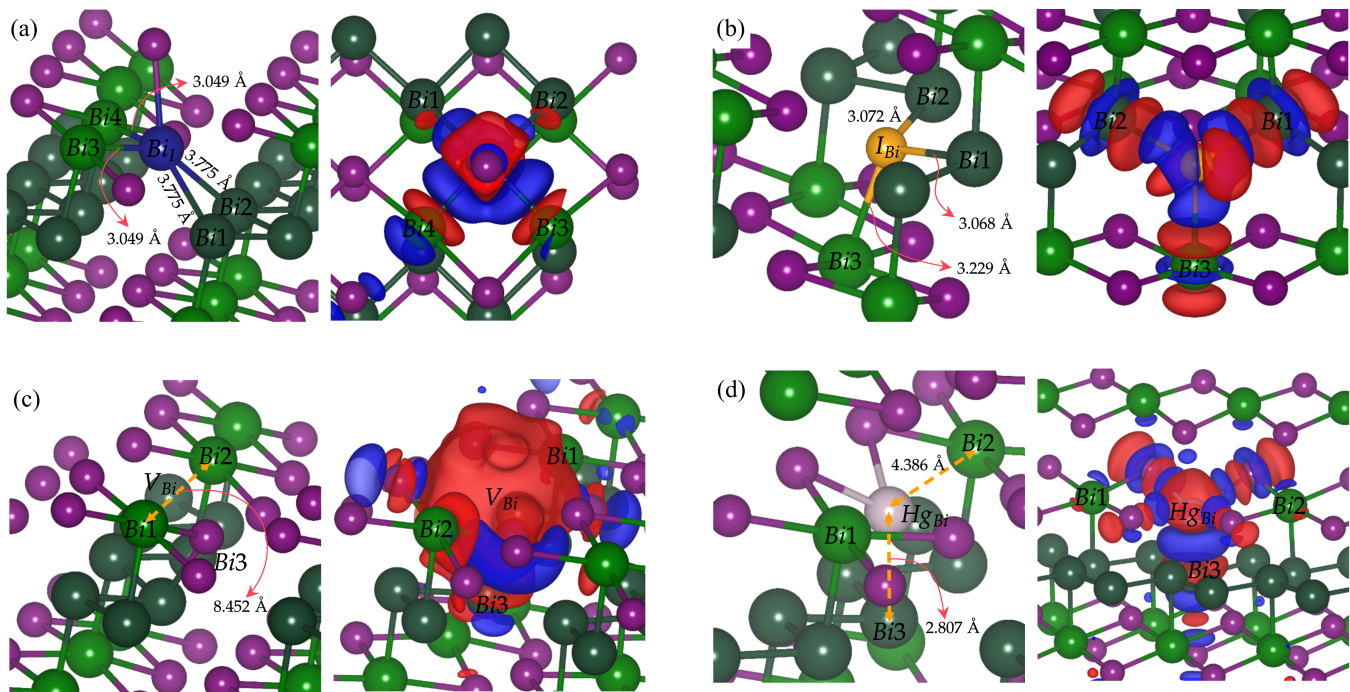


FIG. 4: Relaxed structures and charge density difference isosurfaces of the α phase in the presence of native defects and impurities. In the left panels of (a), (b), (c), and (d) we show the obtained equilibrium geometries of α - Bi_4I_4 in the presence of Bi_i , I_{Bi} , V_{Bi} , and Hg_{Bi} , respectively. Light green and dark green represent the outer and inner bismuth atoms, respectively. Iodine atoms are represented in purple. The corresponding charge density differences are shown in the right panels of (a), (b), (c), and (d). The isosurfaces correspond to $0.001 e/\text{bohr}^3$ charge densities. The red (blue) region denotes electron depletion (accumulation).

bismuth-poor conditions, for the chemical potentials considered. The relaxed structures of the α and β phases in the presence of this type of point defect, shown in Figs. 4(b) and 5(b), indicate a weak local distortion of the chains, which have Bi-I equilibrium bond lengths of 3.07 and 3.23 Å in the α phase. These bond lengths are 3.04 Å ($\text{Bi1-Bi}'$) and 3.07 Å ($\text{Bi3-Bi}'$) in the pristine phases. According to our calculations, we find that the formation of bismuth vacancies is more energetically favorable in Bi-poor conditions than in Bi-rich conditions. Surprisingly, however, they exhibit the second lowest formation energy across the entire chemical potential range. Therefore, without considering competing phases, iodine antisites and bismuth vacancies are expected to be the dominant defects in a bismuth-poor growth condition.

We also studied the case where the existence of competing phases introduce additional limits to bismuth and iodine chemical potentials. As described in the Supplemental Material, we find that the formation energies within these new limits correspond to essentially a region near the Bi-rich conditions, where the bismuth-antisites and bismuth-vacancies are the dominant defects in both phases of Bi_4I_4 . Therefore, the bismuth antisites and vacancies in neutral charge states are expected to be the dominant defects within this narrow energy window of chemical potentials.

C. Formation energies of Hg impurities in Bi-rich growth conditions

Motivated by our EDX results on Hg-grown single crystals, we calculate the formation energies of different configurations of Hg impurities in Bi_4I_4 . Using the supercell approximation we have α - $\text{Bi}_{48}\text{I}_{48}\text{Hg}_1$ and β - $\text{Bi}_{72}\text{I}_{72}\text{Hg}_1$ for the interstitial defects, for instance. The Hg chemical potential was obtained considering the possibility of formation of HgI and HgI_2 phases, and according to our calculations give rise to a Hg-rich condition environment. Table III displays the obtained formation energies of Hg impurities in interstitial and substitutional configurations for both the α and β phases, where several plausible configurations were considered. In this case, we denote Hg substitutional impurities as Hg_{Bi} (Hg_I), and the interstitial impurities as Hg_i .

As can be seen, Hg impurities are energetically favorable to be found at Bi substitutional sites in both α and β phases. At the equilibrium geometries of Hg in α phase [Fig. 4(d)], we find Hg-Bi3 and Hg-Bi2 bond lengths of 2.81 and 4.39 Å, respectively. In the β phase our calculated relaxed structure [Fig. 5(d)] indicates Hg-Bi3 and Hg-Bi2 bond lengths of 2.81 and 4.35 Å, respectively. The corresponding Bi-Bi distances are around 3.07 and 4.4 Å in the pristine phases. The interstitial configuration Hg_i -A(A') formation energies

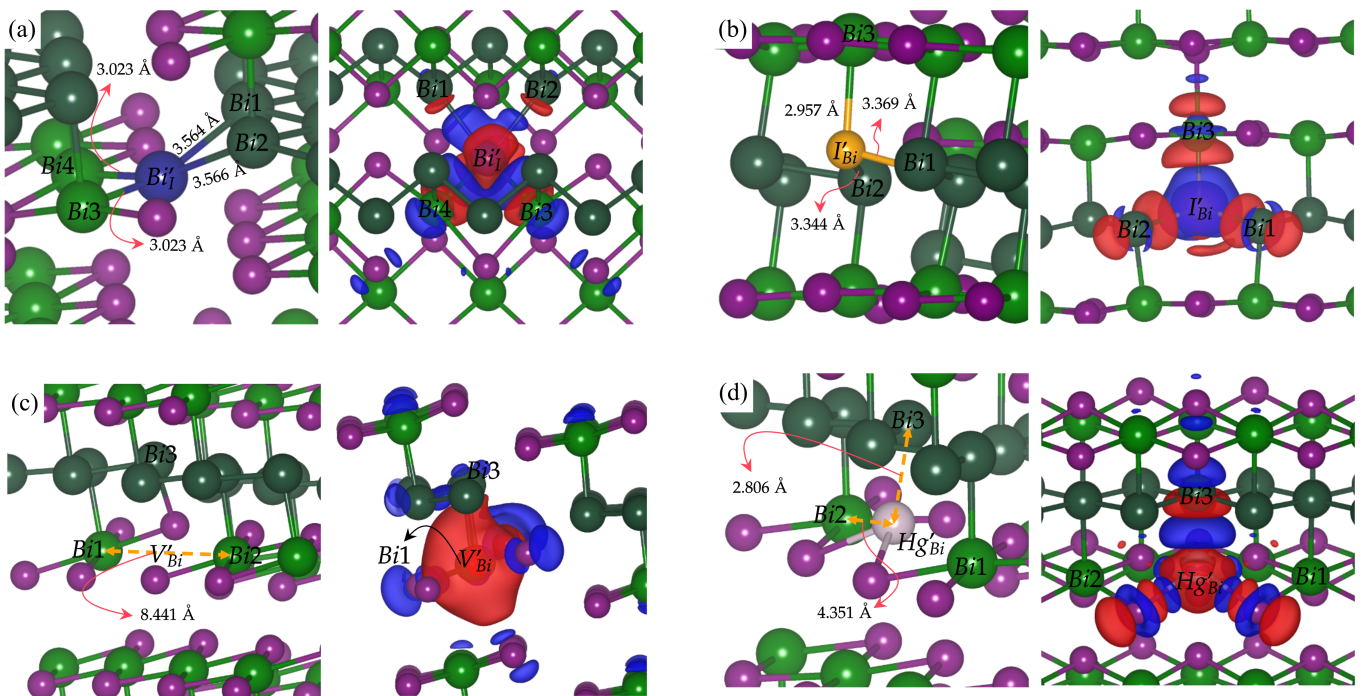


FIG. 5: Relaxed structures and charge density difference isosurfaces of the β phase in the presence of native defects and impurities. In the left panels of (a), (b), (c), and (d) we show the obtained equilibrium geometries of β -Bi₄I₄ in the presence of Bi_I, I_{Bi}, V_{Bi}, and Hg_{Bi}, respectively. Light green and dark green represent the outer and inner bismuth atoms, respectively. Iodine atoms are represented in purple. The corresponding charge density differences are shown in the right panels of (a), (b), (c), and (d). The isosurfaces correspond to 0.001 e/bohr^3 charge densities. The red (blue) region denotes electron depletion (accumulation).

TABLE III: Formation energies (eV), E^f , of neutral Hg impurities in α and β -Bi₄I₄ for Bi-rich (I-poor) conditions.

System	Defect	E^f (eV) Bi-rich
α -Bi ₄ I ₄	Hg _{Bi}	0.47
	Hg _I	0.63
	Hg _i -A	0.98
	Hg _i -B	0.84
β -Bi ₄ I ₄	Hg _{Bi}	0.47
	Hg _I	0.71
	Hg _i -A'	0.63
	Hg _i -B'	0.76

are phase dependent, and are around 0.51 and 0.16 eV higher than the configuration corresponding to Hg at the bismuth sites in the α and β phases, respectively. The Hg configuration in iodine sites has a formation energy of 0.16 eV (0.24 eV) higher than the Hg_{Bi} in the α (β) phase. Thus, our findings indicate that Hg impurities are mostly likely to be found as substitutional impurities at the Bi sites under the Bi-rich condition, as expected due to the similar ionic radius of Hg and Bi. Regarding the structural properties, Hg antisites do not lead to strong local distortions of the chains in both phases.

D. Electronic structure of Bi₄I₄ in the presence of native defects and Hg impurities

The different levels of intrinsic p and n -type doping in Bi₄I₄ are ruled by the relative concentration of native defects and impurities in equilibrium conditions, which can also give rise to additional defect/impurity electronic states, change in charge carrier density and mobility, and to the modulation of the band-edges of Bi₄I₄, and as a result impact the resistivity of Bi₄I₄. In the work of Chen *et al.* [9], it was found that most of their α -Bi₄I₄ samples exhibit intrinsic p -type character, whereas a small number of samples exhibit dominant n -type carriers. According to their quantum transport measurements, in both types of samples, the transport behavior comes from bulk contributions. A small concentration of intrinsic n -type carriers was also observed in photoemission experiments [2] on β -Bi₄I₄. Motivated by those findings and by the variation of the temperature dependence of the electrical resistivity (shown in Fig. 2), we calculate the electronic structure and the local charge density redistribution of both α and β phases in the presence of preferred native defects and Hg impurities. We emphasize here that the DFT(PBE) band gap was used in our analysis; however, it is overestimated in comparison with the ones obtained with the modified Becke-Johnson exchange (mBJ) [3, 20] or

Heyd–Scuseria–Ernzerhof (HSE) functionals [5].

In Figs. 6 and 7 we show the obtained density of states (DOS) and projected density of states (PDOS) for α and β phases in the presence of (a) bismuth and (b) iodine antisites; (c) bismuth vacancies, and (d) Hg antisites. Here, we also used the same labeling for the surrounding atoms, namely, Bi1 and Bi3. The less perturbed Bi atoms were denoted as Bi(int) and Bi(ext). For comparison, we show the pristine bulk DOS (blue lines) in these figures. The red and green dashed lines represent an averaged PDOS of Bi- p and I- p states. Our findings indicate that Bi- p states dominate the Fermi energy’s electronic states.

More importantly, we find that bismuth antisites do not lead to a strong modification of the electronic density of states around the Fermi energy (black lines), though, in the β -phase it modulates the band-edges inducing a small reduction of the band gap. They also do not dope Bi₄I₄, as indicated by the negligible change in the Fermi energy. The corresponding charge redistribution observed in the obtained charge density difference indicates that Bi antisites lead to the accumulation of electrons between Bi_{*l*} and Bi1 and Bi2 atoms, as shown in the right panels of Figs. 4(a) and 5(a), respectively. This charge accumulation is reminiscent of a new interaction between the quasi-1D chains. As shown in the corresponding PDOS, the Bi antisites give rise to resonant electronic states in the valence and conduction band-edges, which may affect the scattering and mobility of charge carriers in Bi₄I₄. The importance of carriers scattering due to resonant states was emphasized in early studies of Sankey and co-workers [21] who studied the electronic scattering in semiconductors with zinc-blende structure. We also mention that charge neutral defects, such as the Bi antisites, can induce carriers scattering due to modifications of the local potential due to structural distortions, as early emphasized in Ref. 22. One can also note that the Bi_{*l*}- p electronic states hybridize with the surrounding iodine and bismuth p states, leading to a considerable contribution to of Bi_{*l*} to the bottom of the conduction band, as can be seen by induced PDOS peaks in Figs. 6(a) and 7(a) (right panels).

Moreover, we observe that the presence of iodine antisites leads to a n -type doping of both the α and β phases, as can be seen in Figs. 6(b) and 7(b), respectively. As can be noticed in the obtained DOS, the Fermi level is located above a region of zero DOS (around -0.25 eV) and indicate that iodine antisites act as donors. In comparison with Bi antisites, the iodine antisites leads a considerable perturbation of the electronic structure of Bi₄I₄, for the considered concentrations associated with our supercell approximation. The largest contribution to the semi-occupied electronic states are due to Bi- p states, from neighbor Bi atoms (Bi3 and Bi1) and from I antisites, as can be seen from the calculated projected density of states. The calculated charge density differences show an accumulation of electrons around the iodine antisites, due to its largest electronegativity and a reduction of electrons between I antisites and

neighbor Bi atoms. On the other hand, a p -type doping is observed for bismuth vacancies, as can be seen in Figs. 6(c) and 7(c). In these cases, the semi-occupied electronic states are mainly due to Bi3- p and Bi(int)- p states near the vacancies. The calculated charge density difference indicate an accumulation of electrons at sites around the vacancies in both phases (as shown by the blue isosurface). Iodine antisites and vacancies introduce semi-occupied states and are expected to act like new scattering centers in Bi₄I₄, also affecting the resistivity during the resistivity measurements.

Finally, we show in Figs. 6(d) and 7(d) the obtained density of states for Bi₄I₄ in the presence of Hg antisites. In this case we find a p -doping of Bi₄I₄, as indicated by the downshift of the Fermi level. The semi-occupied states come mostly from Bi3 and Bi(int)- p states. These defects induce a depletion of electrons at Hg sites and an accumulation of electrons between Hg and neighbor Bi atoms. Thus, Hg antisites lead to the p -type doping of both phases of Bi₄I₄ and to semi-occupied states, which are expected to affect the transport properties.

We summarize the effects of the native defects and Hg antisites in the electronic structure of Bi₄I₄ in Table IV. Overall, our findings indicate that different sorts of defects can give rise to the appearance of different types of doping, semi-occupied electronic states, resonant-states near the valence and conduction band-edges, and a small reduction of the band-gap of Bi₄I₄. In particular, we find that iodine antisites, bismuth vacancies, and Hg impurities can induce the modification of carrier concentration due to charge doping. We expected that these effects can partially explain the electrical resistivity behavior observed for distinct samples of Bi₄I₄. We mention that in a recent theoretical study [23], the authors found that Mn impurities have important effects on the resistivity of Bi₂Te₃, mostly associated with the appearance of impurity states near the Fermi energy, their relative energy position, and the modification of charge carrier concentration. As shown by our calculations these features can be induced by bismuth and iodine antisites, as well as by bismuth vacancies.

We emphasize that these findings are in agreement with the tendency displayed by our resistivity measurements, where the increase in annealing temperature leads to the increase of defect/impurity scattering and to the modification of carrier concentration, which are expected to be the dominant mechanism at low-temperatures. We stress that the quantitative calculations of the electronic scattering due to defects and impurities and its connection with Bi₄I₄ resistivity is beyond the scope of this work. From the experimental side it also requires careful future investigation relating controlled growth conditions with the resulting charge carriers type and crystal quality. The latter investigations are challenging due to the size of the needle-shape Bi₄I₄ crystals, making thin films an interesting platform to be explored for fine-tuning the electronic properties of this compound.

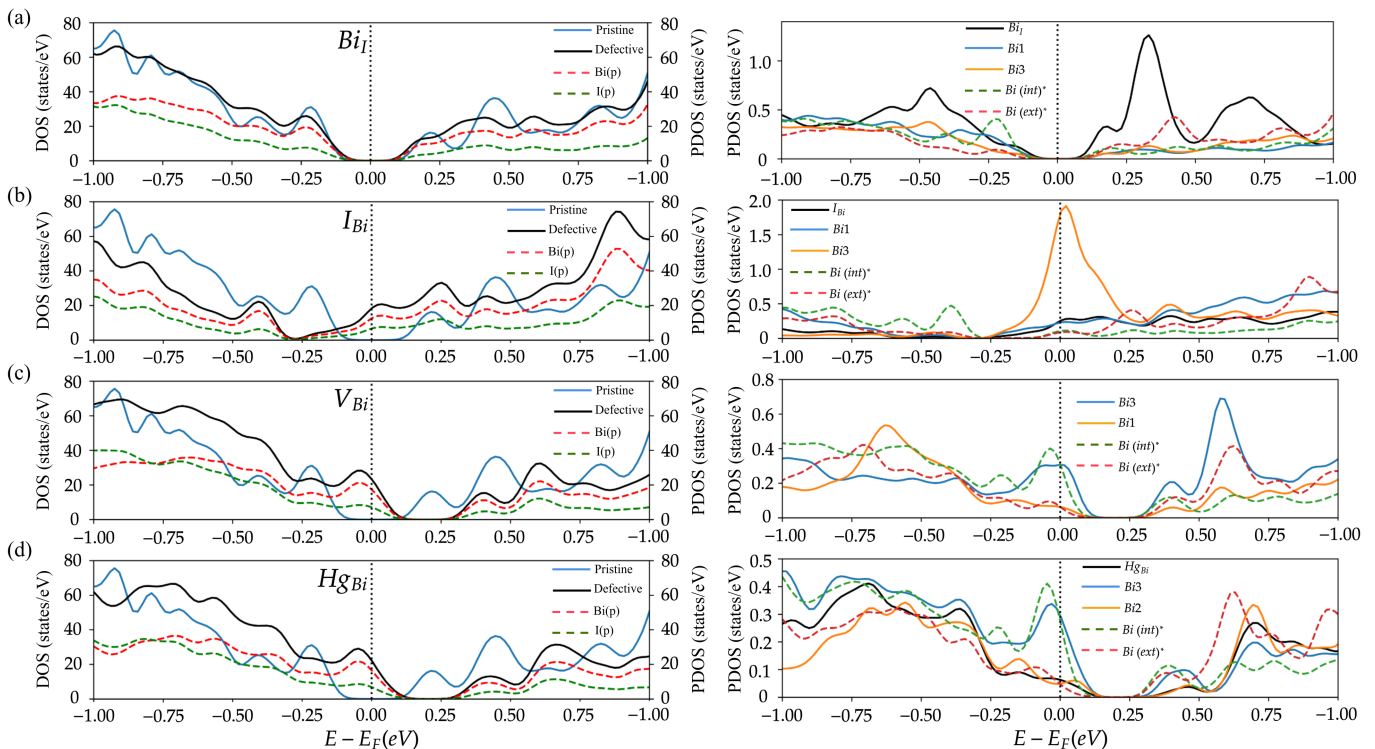


FIG. 6: Total and projected density of states of: (a) bismuth antisite, (b) iodine antisite, (c) bismuth vacancy, and (d) Hg-antisite in α - Bi_4I_4 . The total density of states of the pristine and defective systems are shown in blue and black (left panels), respectively. The projections on the $\text{Bi}(p)$ and $\text{I}(p)$ orbitals are shown in dashed red and green lines (left panels), respectively. The projected densities of states are obtained for the atoms shown in Fig. 4 (right panels).

TABLE IV: Resulting doping type and modulation of band-gap for the most stable point defects on both Bi_4I_4 phases.

System	Defect	Carrier doping	Band gap
α - Bi_4I_4	Bi_I	None	Reduced
	I_Bi	n-type	Closed
	V_Bi	p-type	Closed
	Hg_Bi	p-type	Closed
β - Bi_4I_4	Bi'_I	None	Reduced
	I'_Bi	n-type	Closed
	V'_Bi	p-type	Closed
	Hg'_Bi	p-type	Closed

IV. Conclusions

We have studied the energetics and effects of native defects and Hg impurities on the electronic properties of Bi_4I_4 . We observe that the change of the electrical resistivity of our Bi_4I_4 samples, corresponding to the α phase, can be ascribed by the formation of defects and impurities. By means of DFT calculations we addressed the formation energies and the role of native point defects and Hg impurities on the electronic

properties of both the α and β phases. Regarding the native defects, our findings suggest that bismuth antisites, iodine antisites and bismuth vacancies are the energetically favorable native defects in Bi_4I_4 . The calculated electronic structure indicate that bismuth antisites do not dope the system and leads to a tiny modulation of Bi_4I_4 band-gap and resonant-states in the band-edges. Iodine antisites induce n -type doping while and bismuth vacancies to p -type doping, with the presence of semi-occupied electronic states. Our calculations also suggest that a p -type doping is induced by Hg antisites, with semi-occupied states as well. We expect that these defects and impurities will modify the mobility, carrier density, scattering, and the electrical resistivity of Bi_4I_4 , partially explaining the distinct resistivity profiles of Bi_4I_4 samples.

Acknowledgments

W.H.B. and G.H.C. acknowledge FAPEMIG, CNPq (in particular Grant 402919/2021-1), and the National Laboratory for Scientific Computing (LNCC/MCTI, Brazil) for providing HPC resources of the SDumont supercomputer, which have contributed to the research results, URL: <http://sdumont.lncc.br>. M.C.O.A. acknowledges FAPEMIG, CNPq and CAPES. V.M.

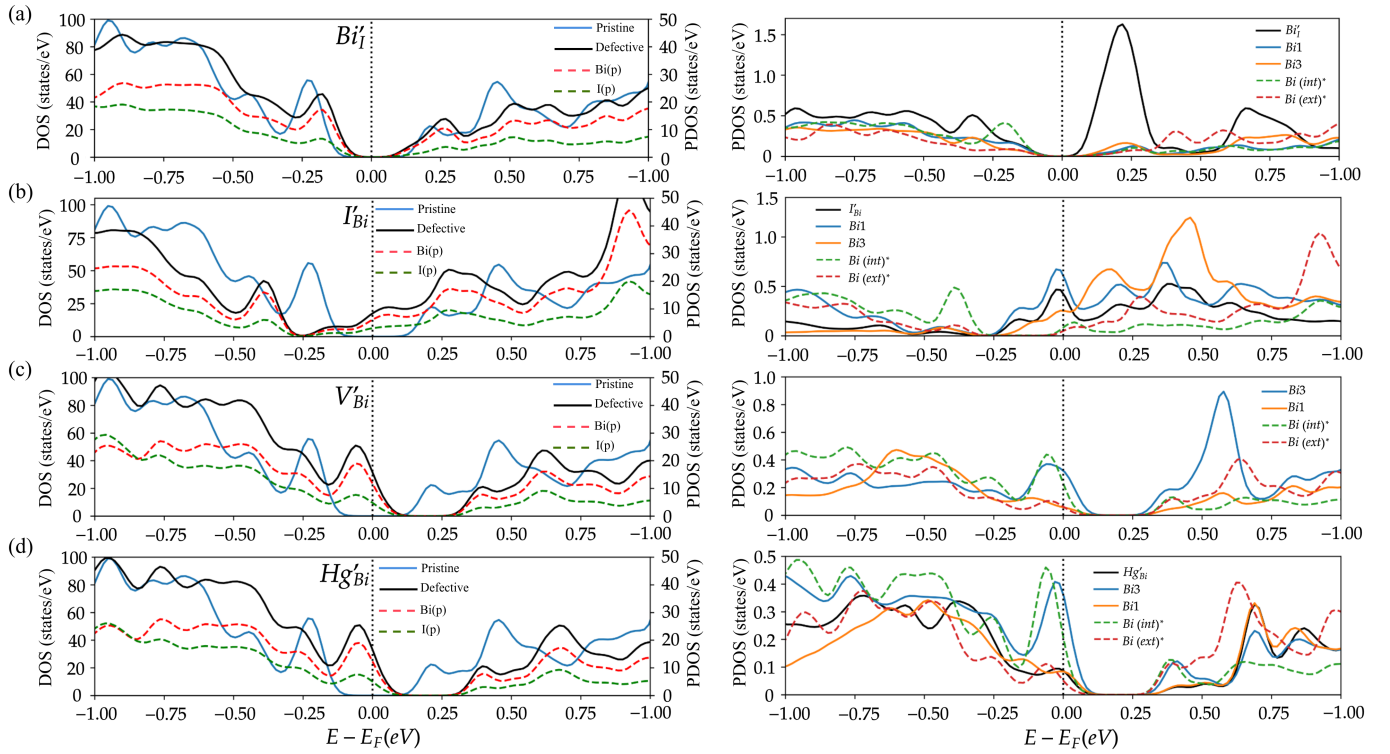


FIG. 7: Total and projected density of states of: (a) bismuth antisite, (b) iodine antisite, (c) bismuth vacancy, and (d) Hg-antisite in β - Bi_4I_4 . The total density of states of the pristine and defective systems are shown in blue and black (left panels), respectively. The projections on the Bi(p) and I(p) orbitals are shown in dashed red and green lines (left panels), respectively. The projected densities of states are obtained for the atoms shown in Fig. 5 (right panels).

and C.D.H. acknowledge FAPESP grants 2018/19420-3, 22/00992-2, 23/11836-4. J. L. J. acknowledges FAPESP JP grant 2018/08845-3 and CNPq Grant

No. 31005/2021-6. The work at the University of Warwick was supported by EPSRC, UK, through Grant EP/T005963/1.

-
- [1] W. X. Junfeng Han and Y. Yao, Quasi-one-dimensional topological material $\text{bi}_4\text{x}_4(\text{x}=\text{br},\text{i})$, *Advances in Physics: X* **7**, 2057234 (2022), <https://doi.org/10.1080/23746149.2022.2057234>.
- [2] G. Autès, A. Isaeva, L. Moreschini, J. C. Johannsen, A. Pisoni, R. Mori, W. Zhang, T. G. Filatova, A. N. Kuznetsov, L. Forró, *et al.*, A novel quasi-one-dimensional topological insulator in bismuth iodide β - bi_4i_4 , *Nature materials* **15**, 154 (2016).
- [3] R. Noguchi, M. Kobayashi, Z. Jiang, K. Kuroda, T. Takahashi, Z. Xu, D. Lee, M. Hirayama, M. Ochi, T. Shirasawa, P. Zhang, C. Lin, C. Bareille, S. Sakuragi, H. Tanaka, S. Kunisada, K. Kurokawa, K. Yaji, A. Harasawa, V. Kandyba, A. Giampietri, A. Barinov, T. K. Kim, C. Cacho, M. Hashimoto, D. Lu, S. Shin, R. Arita, K. Lai, T. Sasagawa, and T. Kondo, Evidence for a higher-order topological insulator in a three-dimensional material built from van der waals stacking of bismuth-halide chains, *Nature Materials* **20**, 473 (2021).
- [4] J. Huang, S. Li, C. Yoon, J. S. Oh, H. Wu, X. Liu, N. Dhale, Y.-F. Zhou, Y. Guo, Y. Zhang, *et al.*, Room-temperature topological phase transition in quasi-one-dimensional material bi_4i_4 , *Physical Review X* **11**, 031042 (2021).
- [5] C.-C. Liu, J.-J. Zhou, Y. Yao, and F. Zhang, Weak topological insulators and composite weyl semimetals: β - bi_4x_4 ($\text{x}=\text{br},\text{i}$), *Physical review letters* **116**, 066801 (2016).
- [6] X. Li, D. Chen, M. Jin, D. Ma, Y. Ge, J. Sun, W. Guo, H. Sun, J. Han, W. Xiao, J. Duan, Q. Wang, C. Liu, R. Zou, J. Cheng, C. Jin, J. Zhou, J. B. Goodenough, J. Zhu, and Y. Yao, Pressure-induced phase transitions and superconductivity in a quasi-1-dimensional topological crystalline insulator α - bi_4br_4 , *Proceedings of the National Academy of Sciences* **116**, 17696 (2019).
- [7] Y. Qi, W. Shi, P. Werner, P. G. Naumov, W. Schnelle, L. Wang, K. G. Rana, S. Parkin, S. A. Medvedev, B. Yan, and C. Felser, Pressure-induced superconductivity and topological quantum phase transitions in a quasi-one-dimensional topological insulator: Bi_4i_4 , *npj Quantum Materials* **3**, 4 (2018).
- [8] S. Deng, X. Song, X. Shao, Q. Li, Y. Xie, C. Chen, and Y. Ma, First-principles study of high-pressure phase

- stability and superconductivity of bi_4i_4 , *Phys. Rev. B* **100**, 224108 (2019).
- [9] D.-Y. Chen, D.-S. Ma, Y. Li, Z. Z. Du, X. Xiong, Y. He, J. X. Duan, J. Han, D. Chen, W. Xiao, and Y. Yao, Quantum transport properties in single crystals of α - bi_4i_4 , *Phys. Rev. Mater.* **2**, 114408 (2018).
- [10] P. Wang, F. Tang, P. Wang, H. Zhu, C.-W. Cho, J. Wang, X. Du, Y. Shao, and L. Zhang, Quantum transport properties of β - bi_4i_4 near and well beyond the extreme quantum limit, *Phys. Rev. B* **103**, 155201 (2021).
- [11] D. Mu, J. Li, Y. Liu, M. Yang, W. Zhou, C. Liu, J. Zhuang, Y. Du, X. Qi, and J. Zhong, Role of hollow defects in lattice phase separation and electronic features in quasi-one-dimensional bi_4i_4 crystals, *The Journal of Physical Chemistry C* **127**, 2098 (2023).
- [12] C. D. Hinostroza, L. Rodrigues de Faria, G. H. Cassemiro, J. Larrea Jiménez, A. Jefferson da Silva Machado, W. H. Brito, and V. Martelli, Structural investigation of the quasi-one-dimensional topological insulator bi_4i_4 , *Phys. Rev. B* **109**, 174105 (2024).
- [13] G. Kresse and J. Furthmüller, Efficiency of ab-initio total energy calculations for metals and semiconductors using a plane-wave basis set, *Computational Materials Science* **6**, 15 (1996).
- [14] G. Kresse and J. Furthmüller, Efficient iterative schemes for ab initio total-energy calculations using a plane-wave basis set, *Phys. Rev. B* **54**, 11169 (1996).
- [15] M. Dion, H. Rydberg, E. Schröder, D. C. Langreth, and B. I. Lundqvist, Van der waals density functional for general geometries, *Phys. Rev. Lett.* **92**, 246401 (2004).
- [16] P. E. Blöchl, Projector augmented-wave method, *Physical review B* **50**, 17953 (1994).
- [17] C. Freysoldt, B. Grabowski, T. Hickel, J. Neugebauer, G. Kresse, A. Janotti, and C. G. Van de Walle, First-principles calculations for point defects in solids, *Reviews of modern physics* **86**, 253 (2014).
- [18] H.-P. Komsa, T. T. Rantala, and A. Pasquarello, Finite-size supercell correction schemes for charged defect calculations, *Physical Review B* **86**, 045112 (2012).
- [19] R. D. Shannon, Revised effective ionic radii and systematic studies of interatomic distances in halides and chalcogenides, *Foundations of Crystallography* **32**, 751 (1976).
- [20] R. Noguchi, T. Takahashi, K. Kuroda, M. Ochi, T. Shirasawa, M. Sakano, C. Bareille, M. Nakayama, M. D. Watson, K. Yaji, A. Harasawa, H. Iwasawa, P. Dudin, T. K. Kim, M. Hoesch, V. Kandyba, A. Giampietri, A. Barinov, S. Shin, R. Arita, T. Sasagawa, and T. Kondo, A weak topological insulator state in quasi-one-dimensional bismuth iodide, *Nature* **566**, 518 (2019).
- [21] O. F. Sankey, J. D. Dow, and K. Hess, Theory of resonant scattering in semiconductors due to impurity central-cell potentials, *Applied Physics Letters* **41**, 664 (1982), https://pubs.aip.org/aip/apl/article-pdf/41/7/664/18447149/664.1_online.pdf.
- [22] V. Gatal'skaya, On the mechanism of charge carrier scattering in germanium with point defects under cyclotron resonance, *Phys. Status Solidi B;(German Democratic Republic)* **133** (1986).
- [23] K. Carva, J. Kudrnovský, F. Máca, V. Drchal, I. Turek, P. Baláz, V. Tkáč, V. Holý, V. Sechovský, and J. Honolka, Electronic and transport properties of the mn-doped topological insulator bi_2te_3 : A first-principles study, *Phys. Rev. B* **93**, 214409 (2016).